Article

Morphologies of Star-Block Copolymers in Dilute Solutions

Yu-Jane Sheng, Chih-Hsiung Nung, and Heng-Kwong Tsao

J. Phys. Chem. B, **2006**, 110 (43), 21643-21650 • DOI: 10.1021/jp0642950

Morphologies of Star-Block Copolymers in Dilute Solutions

Yu-Jane Sheng,[†,‡] Chih-Hsiung Nung,[†] and Heng-Kwong Tsao*[,§]

Department of Chemical Engineering and Institute of Polymer Science and Engineering, National Taiwan University, Taipei, Taiwan 106, Republic of China, and Department of Chemical and Materials Engineering, National Central University, Jhongli City, Taiwan 320, Republic of China

Received: July 7, 2006; In Final Form: August 21, 2006

The morphologies of star-block copolymer $(AB)_n$ and $(BA)_n$ in a selective solvent for *A*-block are investigated by using dissipative particle dynamics. For a star-block copolymer of $(BA)_n$ type with a large enough arm number *n*, since the solvophobic *B*-blocks are situated in the inner part of the star, it behaves as a unimolecular micelle with the *B*-block core and *A*-block hairy corona. These types of star copolymers repel each other, thus it is quite difficult to form multimolecular micelles. On the other hand, for a star-block copolymer of $(AB)_n$ type, a few aggregative domains develop on the outer rim of the molecule. As the length of *B*-blocks or the repulsive interaction between *B*-blocks and solvents is increased, the tendency of *B*-blocks to associate within the star increases and thus the average number of aggregative domains declines. Owing to the exposure of *B*-domains, $(AB)_n$ type star-blocks tend to form micelles with morphology different from typical micelles. Upon performing simulations for solutions with multiple stars, we have shown that the single molecular conformation may greatly affect the resulting morphology of the supramolecular structure, such as connected-star aggregate, multicore micelle, segmented worm, and core-lump micelle.

I. Introduction

Star-shape block copolymers possess the ability to exhibit different morphologies in polymer solutions, in the bulk state as well as in thin layers at surfaces and interfaces due to their complex architecture. This unique property allows them to become potential materials for many modern applications such as nanocarriers for drug delivery[1−3] and fabrication of smart polymer films.[4] Various molecular architectures of star copolymers have been reported,[5−9] including heteroarm A_nB_n, miktoarm A_nB_m, and star-block $(AB)_n$ structures. For heteroarm and miktoarm diblock star polymers, two different kinds of arms emanate from the same core. Each arm is composed of only *A*- or *B*-type units. A heteroarm star copolymer bears an equal number of *A* and *B* arms such as polystyrene/poly(2-vinylpyridine) (PS_7-PVP_7) while a miktoarm star has asymmetric *A* and *B* arms. On the other hand, a star-block copolymer $(AB)_n$ is composed of *n* diblock arms with an *A* (or *B*) block as the inner section of the arms. Examples include poly(*tert*-butyl acrylate)/poly(methyl methacrylate), (PtBA-*b*-PMMA)$_{12}$, and polystyrene/polyisoprene, (PS-*b*-PI)$_{18}$.[10,11]

When linear diblock copolymers are dissolved in a solvent selective for one constituent, in most cases they may self-assemble to form spherical micelles that consist of a core formed by insoluble blocks surrounded by a shell of the solvated blocks. Recently, it has been reported that star copolymers are also associated to form micelles. However, differences in the micellization properties between star and linear diblock copolymer were observed.[12,13] For example, the critical micelle concentration (cmc) of the heteroarm star copolymer is much higher than that observed for the linear copolymer. The cmc of PS_6-PVP_6 in toluene is 7.4×10^{-4} g/cm^3, while that of the linear copolymer having the same block length is 2.2×10^{-7} g/cm^3, 3 orders of magnitude lower.[12] In the selective solvent dimethylacetamide, the star-block copolymers (PS-*b*-PI)$_8$ were found to form micelles of smaller size, having lower aggregation number and shorter coronas compared to those of the linear diblock copolymer (PS-*b*-PI) with similar composition and molecular weight.[13] This consequence indicates that the difference in architecture between star and linear copolymers results naturally in diverse molecular conformations and therefore their solution behavior.

Block copolymers can self-organize into a wide variety of supramolecular assemblies. Single molecular conformations associated with a block copolymer in different solvent qualities play an essential role in determining the aggregation behavior and supramolecular structures. Most of the investigations on morphology of structures formed by macromolecules in solutions were inferred from scattering techniques, viscometry, or cryo-transmission electron microscopy. However, details of morphology cannot be easily extracted for molecules with complex structures. Recently, single molecular morphologies of heteroarm star copolymers were investigated by atomic force microscopy (AFM) with molecular resolution.[14,15] Assuming that the adsorbed molecules still preserve their conformations formed in solutions, PS_7-PVP_7 was deposited onto mica or Si wafers from different solvent conditions. The experimental results revealed that even the solvent (*S*) is good for both *A*- and *B*-blocks of a star copolymer; differences in affinity between *A*−*S* and *B*−*S* induce an intramolecular segregation, leading to the formation of "Janus"-like conformation. On the contrary, a near-uniform spherical structure is present as the attraction between *A*−*S* and *B*−*S* becomes comparable. Those works provide us with insightful information of possible conformations associated with heteroarm star copolymers in solutions. Nevertheless, these findings were based on speculation from the observed "hat-like" and "spherical" conformations of the

[†] Department of Chemical Engineering, National Taiwan University.
[‡] Institute of Polymer Science and Engineering, National Taiwan University.
[§] National Central University.

10.1021/jp0642950 CCC: $33.50
Published on Web 10/07/2006

adsorbed star copolymers. It is still uncertain whether the polymer conformation in solution is preserved after deposition.

An alternative for studying macromolecular features that are not fully accounted for by experiments is molecular simulation. Monte Carlo (MC) simulations have been carried out for homoarm star polymers and gave important insight in developing the scaling relations of conformational properties.[16,17] The conformational properties of miktoarm star copolymers in dilute solutions were investigated and the simulation results were used to examine the validity of certain theoretical models.[18] Recently, conformations of heteroarm star copolymer in good and selective solvents were studied by lattice MC simulations. In strongly selective solvents, the possibility of formation of nonspherical structures was suggested.[19] We have also performed off-lattice MC simulation to analyze conformations of heteroarm star copolymers. Intramolecular segregation is always observed in selective solvents and the degree of segregation grows with increasing arm numbers.[20] According to the second virial coefficient calculation, the intramolecular Janus segregation can lead to intermolecular attractions.

In this work, we investigate morphologies of $(AB)_n$ and $(BA)_n$ type star-block copolymers in a selective solvent for *A*-block by using dissipative particle dynamics, which is a mesoscopic simulation method. For single molecular morphology, we focus on intramolecular segregation phenomena due to incompatibility between different block types as well as selective solvents. The effects of block length and interaction between *B*-block and solvent on the degree of intramolecular segregation are studied. To understand the influence of single molecular conformation on the supramolecular morphology, simulations for dilute solutions with multiple star-blocks are performed. Various supramolecular morphologies which differ from typical core-corona micelles are observed, including multicore micelle, segmented-worm, and core-lump micelle.

II. Model and Simulation Methods

We intend to study the characteristics of the conformations associated with a single star-block copolymer and morphologies of supramolecules formed by multiple stars. Current experimental techniques can only provide indirect evidence for their conjecture of the morphology. Molecular simulations, on the other hand, can make microscopic detailed structures available and thus allow us to understand the conformational properties without any speculation. The building of mesoscale micellar solutions with the use of classical molecular dynamics (MD) simulations at atomic resolution is a challenge at present owing to the length and time scales at which these phenomena can occur. On the other hand, mesoscopic simulations, such as dissipative particle dynamics (DPD), can treat a wider range of length and time scales by many orders of magnitude compared to atomistic simulations. In this study we perform dissipative particle dynamics (DPD)[21−23] to explore the morphological characteristics of star-block copolymers in dilute solutions.

The DPD method, introduced by Hoogerbrugge and Koelman in 1992,[21] is a particle-based, mesoscale simulation technique. This method combines some of the detailed description of MD but allows the simulation of hydrodynamic behavior in much larger and more complex systems, up to the microsecond range. In a DPD simulation, a particle having mass m represents a block or cluster of atoms or molecules moving together in a coherent fashion. These DPD particles are subject to soft potentials and governed by predefined collision rules. Like MD, the DPD particles obey Newton's equation of motion,

$$\frac{d\mathbf{r}_i}{dt} = \mathbf{v}_i, \qquad \frac{d\mathbf{v}_i}{dt} = \mathbf{f}_i \tag{1}$$

where $\mathbf{f}_i$ denotes the total forces acting on particle i. In the system, there are three different species of DPD particles, including solvent (*S*), solvophilic particle (*A*), and solvophobic particle (*B*).

The force is composed of three different pairwise-additive forces: conservative ($\mathbf{F}^C$), dissipative ($\mathbf{F}^D$), and random forces ($\mathbf{F}^R$),

$$\mathbf{f}_i = \sum_{j\neq i}(\mathbf{F}_{ij}^C + \mathbf{F}_{ij}^D + \mathbf{F}_{ij}^R) \tag{2}$$

These forces conserve net momentum and all act along the line joining the two particles. The conservative force $\mathbf{F}^C$ for nonbonded beads is a soft repulsive force,

$$\mathbf{F}_{ij}^C = \begin{cases} a_{ij}(1 - r_{ij})\hat{\mathbf{r}}_{ij} & r_{ij} < 1 \\ 0 & r_{ij} > 1 \end{cases} \tag{3}$$

where a_{ij} is a maximum repulsion between particles i and j and r_{ij} is the magnitude of the bead−bead vector. $\hat{\mathbf{r}}_{ij}$ is the unit vector joining beads i and j. The relationship between a and the Flory−Huggins parameter χ has been established by Groot and Warren,[23] $a_{ij} = a_{ii} + 3.497\chi_{ij}$ for density $\rho = 3$. For bonded beads on the star copolymers, the interaction force is

$$\mathbf{F}_{i,\text{spring}}^C = -\sum_j C(r_{ij} - r_{\text{eq}})\hat{\mathbf{r}}_{ij} \tag{4}$$

where the sum runs over all particles to which particle i is connected. In this work, we have chosen $C = 100$ and $r_{\text{eq}} = 0.7$. This choice is only a coarse-graining selection to show the constraint imposed upon connected beads of a polymeric chain. It is not meant to correspond to a certain realistic star-block copolymer. Also, this choice of C and r_{eq} will not affect the qualitative behavior of the systems studied in our work. The dissipative or drag force has the form,

$$\mathbf{F}_{ij}^D = -\gamma w^D(r_{ij})(\hat{\mathbf{r}}_{ij}\cdot\mathbf{v}_{ij})\hat{\mathbf{r}}_{ij} \tag{5}$$

where $\mathbf{v}_{ij} = \mathbf{v}_i - \mathbf{v}_j$ and w^D is an r-dependent weight function. The form is chosen to conserve the total momentum of each pair of particles and therefore the total momentum of the system is conserved. The dissipative force acts to reduce the relative momentum between particles i and j, while random force is to impel energy into the system. The random force also acts between all pairs of particles as

$$\mathbf{F}_{ij}^R = \sigma w^R(r_{ij})\theta_{ij}\hat{\mathbf{r}}_{ij} \tag{6}$$

where w^R is also an r-dependent weight function and θ_{ij} is a randomly fluctuating variable with Gaussian statistics:

$$\langle\theta_{ij}(t)\rangle = 0, \qquad \langle\theta_{ij}(t)\theta_{kl}(t')\rangle = (\delta_{ik}\delta_{jl} + \delta_{il}\delta_{jk})\delta(t - t') \tag{7}$$

Note that in Brownian dynamics white noise is added to the equation of motion for each particle independently. However, in DPD simulation, the random force is acting along the line of center of each pair of beads and therefore conserves the total momentum even as it puts in energy to the system. Espagñol and Warren[22] have shown that in order to satisfy the fluctuation−dissipation theorem and for the system to evolve to a steady state that corresponds to the Gibbs Canonical ensemble, only one of the two weight functions can be chosen arbitrarily

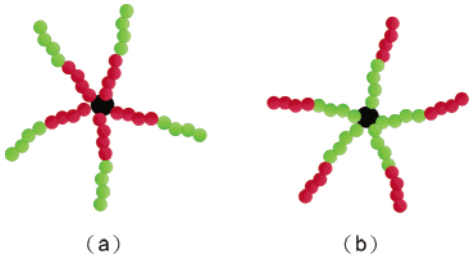

Figure 1. Schematic representations of star-block copolymers (a) $(BA)_n$ type and (b) $(AB)_n$ type. The green bead represents solvophilic *A* and red bead denotes solvophobic *B*. The black bead is the center of the star.

TABLE 1: Maximum Repulsion between Bead *i* and Bead *j*

a_{ij}	*A*	*B*	*S*[a]
A	25	45	26
B	45	25	35
S	26	35	25

[a] *S* represents the solvent of the system.

and this choice fixes another weight function. There is also a relationship between the amplitudes (σ and γ) and k_BT. Therefore,

$$w^D(r) = [w^R(r)]^2$$
$$\sigma^2 = 2\gamma k_B T \tag{8}$$

According to Groot and Warren,[23] we choose

$$w^D(r) = [w^R(r)]^2 = \begin{cases} (1-r)^2 & r < 1 \\ 0 & r \geq 1 \end{cases} \tag{9}$$

The masses of the beads are set as 1, therefore the force acting on a bead equals its acceleration. Also, as we can see, all the forces except for the bonded spring force come to zero outside a certain cutoff radius r_c, where $r_c = 1$ in this work.

A modified version of the velocity-Verlet algorithm is used here:[23]

$$\mathbf{r}_i(t+\Delta t) = \mathbf{r}_i(t) + \Delta t \mathbf{v}_i(t) + \frac{1}{2}(\Delta t)^2 \mathbf{f}_i(t)$$
$$\tilde{\mathbf{v}}_i(t+\Delta t) = \mathbf{v}_i(t) + \lambda \Delta t \mathbf{f}_i(t)$$
$$\mathbf{f}_i(t+\Delta t) = \mathbf{f}_i(\mathbf{r}(t+\Delta t), \tilde{\mathbf{v}}(t+\Delta t))$$
$$\mathbf{v}_i(t+\Delta t) = \mathbf{v}_i(t) + \frac{1}{2}\Delta t(\mathbf{f}_i(t) + \mathbf{f}_i(t+\Delta t)) \tag{10}$$

Note that for $\lambda = 0.5$, the actual velocity-Verlet algorithm is recovered. Here, we choose $\lambda = 0.65$ because for this value of λ, Groot and Warren[23] found that the time step can be increased to $\Delta t = 0.06$ without significant loss of temperature control.

On the basis of the algorithm described, we simulate the single molecular conformations and supramolecular morphologies associated with the $(AB)_n$ and $(BA)_n$ type star-block copolymers, as illustrated in Figure 1. For a star-block copolymer, there are *n* arms. The *AB* diblock arm consists of L_A *A*-beads and L_B *B*-beads. The maximum repulsions between beads *i* and *j* are listed in Table 1. The systems are set at $\rho = 3$ in a cubic box of size L^3 with *L* varying from 20 to 40. A total of 10^5 time steps with step size $\Delta t = 0.05$ are performed for equilibration. Afterward that the resulting morphologies are analyzed.

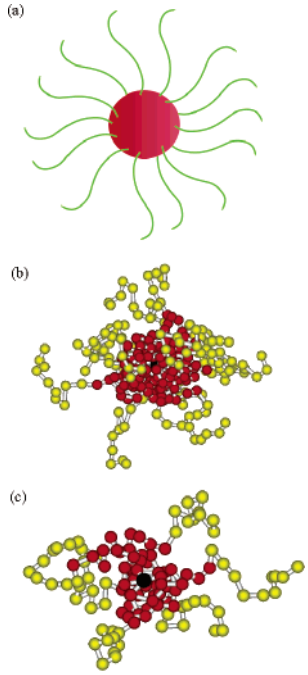

Figure 2. A unimolecular micelle of a $(BA)_n$ star-block copolymer in a selective solvent for *A*-block ($L_A = L_B = 10$). (a) Schematic representation for $n = 14$ star-block copolymer. (b) Snapshot obtained from simulation for $n = 14$ star-block copolymer. (c) Snapshot obtained from simulation for $n = 6$ star-block copolymer.

III. Results and Discussion

The conformations of single star-block copolymer $(BA)_n$ and $(AB)_n$ in a selective solvent are studied by DPD simulations. The solvent is good for *A*-block but poor for *B*-block. The intramolecular segregation is then induced and leads to various single molecular morphologies. The effects of block length and interaction between *B*-block and solvent are examined. They may greatly affect the interactions between two star-block copolymers, which then influence the morphologies of supramolecules. DPD simulations for solutions with multiple star-block copolymers are then performed to investigate supramolecular morphologies.

1. Single Star-Block Conformation. In a selective solvent for *A*-block, the intramolecular segregation is induced for both $(AB)_n$ and $(BA)_n$ type star-block copolymers owing to effective attractions among *B*-blocks. Note that all DPD beads are interacted through repulsive interactions. However, the resulting conformations are quite different for these two types of stars.

a. $(BA)_n$ *Type Star-Block.* For $(BA)_n$ star, the *B*-block is situated in the inner part of the arm (near the center). As a result, in a selective solvent, the *B*-blocks attract each other and collapse into a core. This solvophobic core is then surrounded by the solvophilic *A*-blocks, which form the hairy corona, as shown in parts a and b of Figure 2 for $n = 14$. Evidently, the single molecular morphology of the $(BA)_n$ star-block copolymer is very similar to the micelle self-assembled by linear *AB* diblock copolymers. However, there are significant differences between them. The former is a unimolecular micelle, which can exist in very dilute solution, and the aggregation number is simply the arm number. For typical micelles, the constituent linear diblock copolymers constantly exchange themselves between micelles and solution. The unimolecular micelle cannot participate in

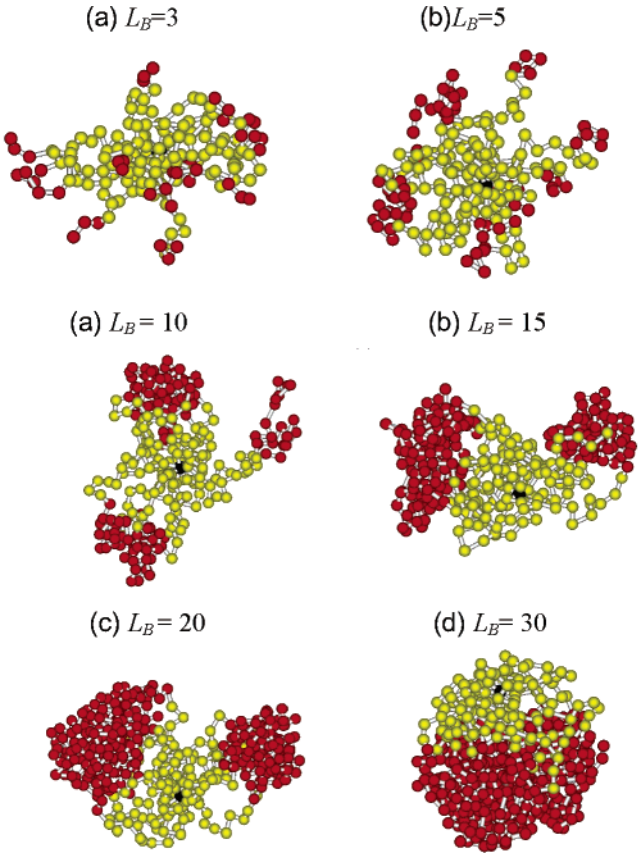

Figure 3. Single molecular conformations of $(AB)_{14}$ star-block copolymer in a selective solvent with fixed *A*-block length ($L_A = 10$) and variant *B*-block length: (a) $L_B = 3$; (b) $L_B = 5$; (c) $L_B = 10$; (d) $L_B = 15$; (e) $L_B = 20$; and (g) $L_B = 30$. The black bead represents the center of the star-block copolymer.

such a dynamic equilibrium process because the individual diblocks are covalently bound together. For $(BA)_n$ type star-block copolymers with large enough *n*, it is difficult to develop multimolecular micelles owing to the repulsion between two stars' coronas formed by *A*-blocks. However, if *n* is small, there are no sufficient *A*-blocks to effectively protect the *B*-block core as shown in Figure 2c. The probability for *B*-block cores to contact and collapse into one is increased. Therefore, there is a great chance for multimolecular micelle to form.

b. $(AB)_n$ *Type Star-Block.* For a single $(AB)_n$ type star-block in a selective solvent, the outer block is solvophobic. To reduce the contact with solvent, aggregative domains formed by *B*-blocks are developed on the outer rim of the star. The extent of aggregation depends on the *B*-block length (L_B) and is essentially the consequence of the competition between monomer−monomer attraction and conformational entropy of the polymer. As one can see from Figure 3, when $L_B = 3$, the tendency for *B*-block to aggregate is weak. This is due to the fact that the energy gain of aggregation cannot compete with the entropic dispersion within the star. Therefore all the arms assume the dispersed conformation as illustrated in Figure 3a. As L_B is increased, the number of aggregative domains declines but the size associated with the domain rises, as is clearly shown in Figures 3b−f. These results indicate that the energy effect becomes comparable and then gradually dominant over entropic one. Finally the star-block takes up the Janus conformation. In other words, the energy associated with *B*−*B* attractions and *B*−*S* repulsions overwhelms the entropy associated with dispersive conformations. Thus, *B*-blocks tend to exclude *A*-blocks and collapse into a globule to reduce the contacts with the solvents. As depicted in Figure 3f, the northern hemisphere is solvophilic and the southern is solvophobic.

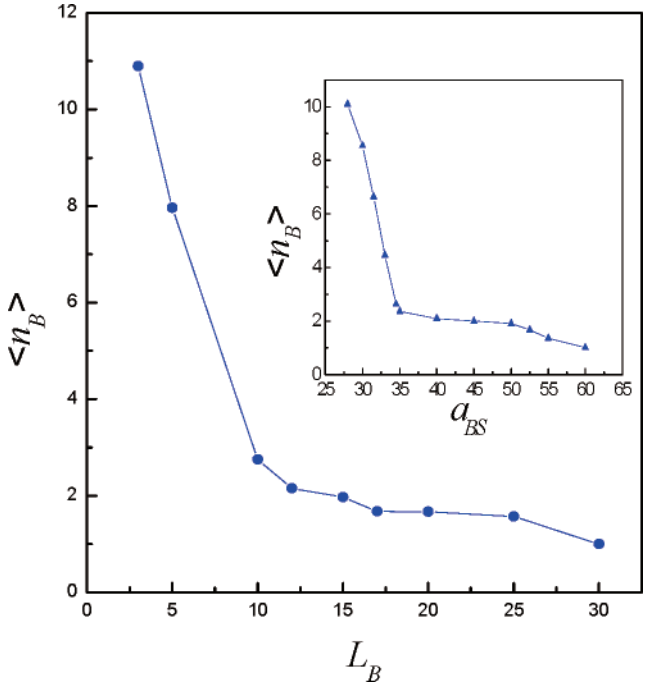

Figure 4. The variation of average number of *B* domains $\langle n_B \rangle$ with *B*-block length (L_B) for $(AB)_{14}$ star-block with $L_A = 10$ and $a_{BS} = 35$. The inset shows $\langle n_B \rangle$ versus a_{BS} for $(AB)_{14}$ star-block with $L_A = L_B = 10$.

Figure 4 shows the variation of the average number of *B* domains $\langle n_B \rangle$ with L_B for $(AB)_{14}$ star-block with $L_A = 10$. The average number of *B* domains drops fairly quickly as *B*-block length (L_B) increases and the size of the aggregative domain increases accordingly. Note that although for $L_B = 15-25$ there are approximately two domains formed by *B*-blocks, the system is actually in dynamic equilibrium. We have observed arms switching between the two domains. When the *B*-block length is long enough, all *B*-blocks favor a collapse into one domain and the intramolecular Janus segregation is observed. The entropy associated *A*-blocks are sacrificed in such a Janus conformation. The exposure of the *B*-domains to the solvents indicates that a star-block with long solvophobic blocks is not stable and tends to form aggregates with other star-blocks. It is worth mentioning that the transition from multiple-domain to single-domain is not a sharp, first-order transition. The crossover L_B value depends on many factors such as arm number, arm length of *A*, and interactions between *AB*, *BS*, etc. In this study, it is quite clear that the crossover L_B value for the collapse of the *B* blocks into single domains lies between 25 and 30 (Figure 4).

Within a star-block copolymer, the segregation of *A*- and *B*-blocks into distinct domains requires strong effective repulsion between the two blocks. The segregation strength in polymers is typically quantified by the dimensionless product χN, where χ denotes the monomer−monomer interaction parameter (related to a_{BS} and a_{AB}) and *N* is the degree of polymerization. Consequently, the conformation change from a dispersed limit to a Janus limit can also be achieved for a $(AB)_n$ type star-block with $L_A = L_B = 10$ by varying the repulsive interaction parameter between the *B* monomer and solvent bead, i.e., a_{BS}. As *B*-block becomes more and more solvophobic, the tendency of *B*-blocks to aggregate to avoid contacting with solvents grows stronger. As shown in the inset of Figure 4, the variation of the average number of *B* domains versus a_{BS} behaves quite similar

to that of $\langle n_B \rangle$ versus L_B. These results indicate that we can achieve the task of controlling the conformation of a single star-block copolymer by adjusting the length of the solvophobic block or by altering the solvent.

2. Supramolecular Morphologies. It is generally anticipated that diblock copolymers in a selective solvent will self-assemble into micelles as its concentration exceeds the critical micelle concentration. However, it is not necessarily true for star-block copolymers. Moreover, the supramolecular morphologies of the multiple star-block copolymers in dilute solutions may be greatly influenced by the corresponding single molecular conformations.

a. $(BA)_n$ *Type Star-Block.* A unimolecular micelle is observed for a $(BA)_{14}$ star-block in a selective solvent. Since the *B*-block length is long enough (cf. χN), all inner *B*-blocks in a star form a solvophobic core. However, the outer, solvophilic *A*-blocks give rise to the hairy corona, which offers steric protection and prevents the contact between two *B*-block cores. According to our previous Monte Carlo study,[20] owing to the excluded-volume interactions provided by the extended shell of hairy arms, the effective interaction potential between two $(BA)_{14}$ stars is always repulsive as indicated by the second virial coefficient. As a consequence, it is expected to be rather difficult for $(BA)_{14}$ star-blocks possessing a unimolecular micelle conformation to form supramolecular micelles. Our simulation result for multiple $(BA)_{14}$ star-blocks confirms the expectation and agrees with the experimental observation of (PI-*b*-PS)$_8$ in ethyl acetate by static light scattering.[13] In Figure 5a, we can clearly see that the $(BA)_{14}$ star-blocks form randomly dispersed unimolecular micelles.

Previous experimental study[13] ((PS-*b*-PI)$_8$ in dimethylacetamide) and Brownian dynamics (BD) simulation[24] ($n \leq 9$) show that multimolecular micelles may be formed by $(BA)_n$ star-blocks although its aggregation number is much smaller than that associated with linear *BA* diblock copolymers. Note that arm numbers $n = 1$ and 2 correspond to respectively *AB* diblock and *ABA* triblock copolymers, which will form micelles in a selective solvent. The BD simulation indicates that the average aggregation number is inversely proportional to the arm number. Also, in the BD simulation, the average aggregation number is less than two for about $n \geq 8$.[24] Our simulation results show a similar trend. The average aggregation number becomes less than two for $n \geq 10$. This consequence reveals that $(BA)_n$ star-blocks with large enough n are difficult to self-assemble. In Figure 5a, the arm number is quite high, i.e., $n = 14$. Therefore, the $(BA)_{14}$ star-block is essentially a unimolecular micelle, which is stable and resists forming an aggregate with other star-blocks. However, for a dilute solution of $(BA)_6$ star-blocks, several multimolecular micelles exist in the solution as shown in Figure 5b. As we have mentioned earlier, $(BA)_n$ star-blocks with only a few arms do not possess adequate *A*-blocks to form a protective layer to shield the *B*-block core. Therefore, *B*-block cores tend to aggregate to form multimolecular micelles. Note that the changeover from multimolecular to unimolecular micelle is believed not to be a sharp, first-order transition but a smooth crossover.

As to the multimolecular micelles formed by (PI-*b*-PS)$_8$ in dimethylacetamide, a plausible explanation is that the solvent is close to θ solvent for the outer PS-block. In our simulation, we have clearly observed the formation of multimolecular micelles for $(BA)_{14}$ star-blocks by adjusting a_{AS} from 26 and 28. Since the solvents become less favorable for *A*, the interaction between $A-A$ blocks becomes more attractive. As a result, *A*-blocks do not provide strong enough steric hindrance between two stars. It is easier for two *B*-block cores to contact.

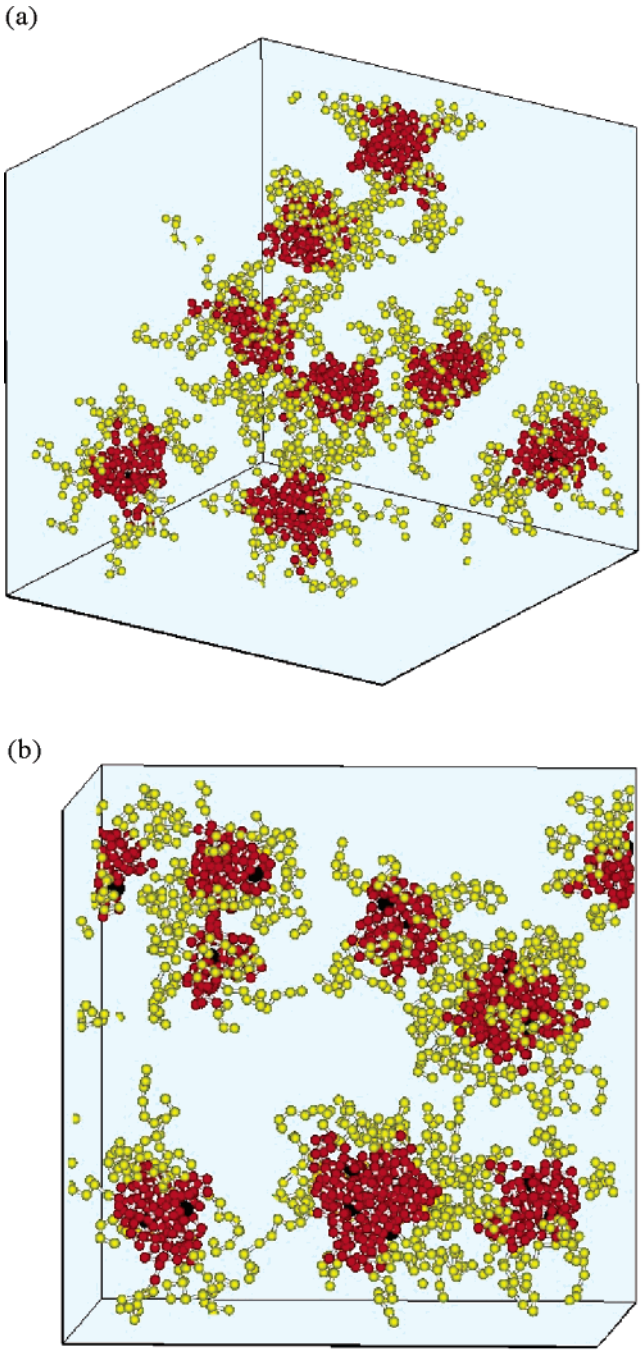

Figure 5. Morphology of multiple $(BA)_n$ type star-block copolymers in a selective solvent. $L_A = L_B = 10$ and volume fraction = 0.05. (a) $n = 14$ (only unimolecular micelles exist) and (b) $n = 6$ (multimolecular micelles can be observed).

Instead of unimolecular micelles, multimolecular micelles may prevail in the solution.

b. $(AB)_n$ *Type Star-Block.* Unlike $(BA)_n$ stars, $(AB)_n$ stars display various single molecular conformations as the length of the solvophobic *B*-block (L_B) increases. This consequence results in diverse supramolecular morphologies. As we have seen in Figure 3 for $L_A = 10$, the outer blocks are solvophobic and tend to develop aggregative domains on the periphery of a $(AB)_n$ type star-block. Those solvophobic nanodomains may serve as junction locations for forming multimolecular micelles. Depending on the number of nanodomains, different supramolecular morphologies may be generated.

For *B*-block length $L_B = 3$, the entropic effect within the star-block dominates over the energetic one, thus arms of a

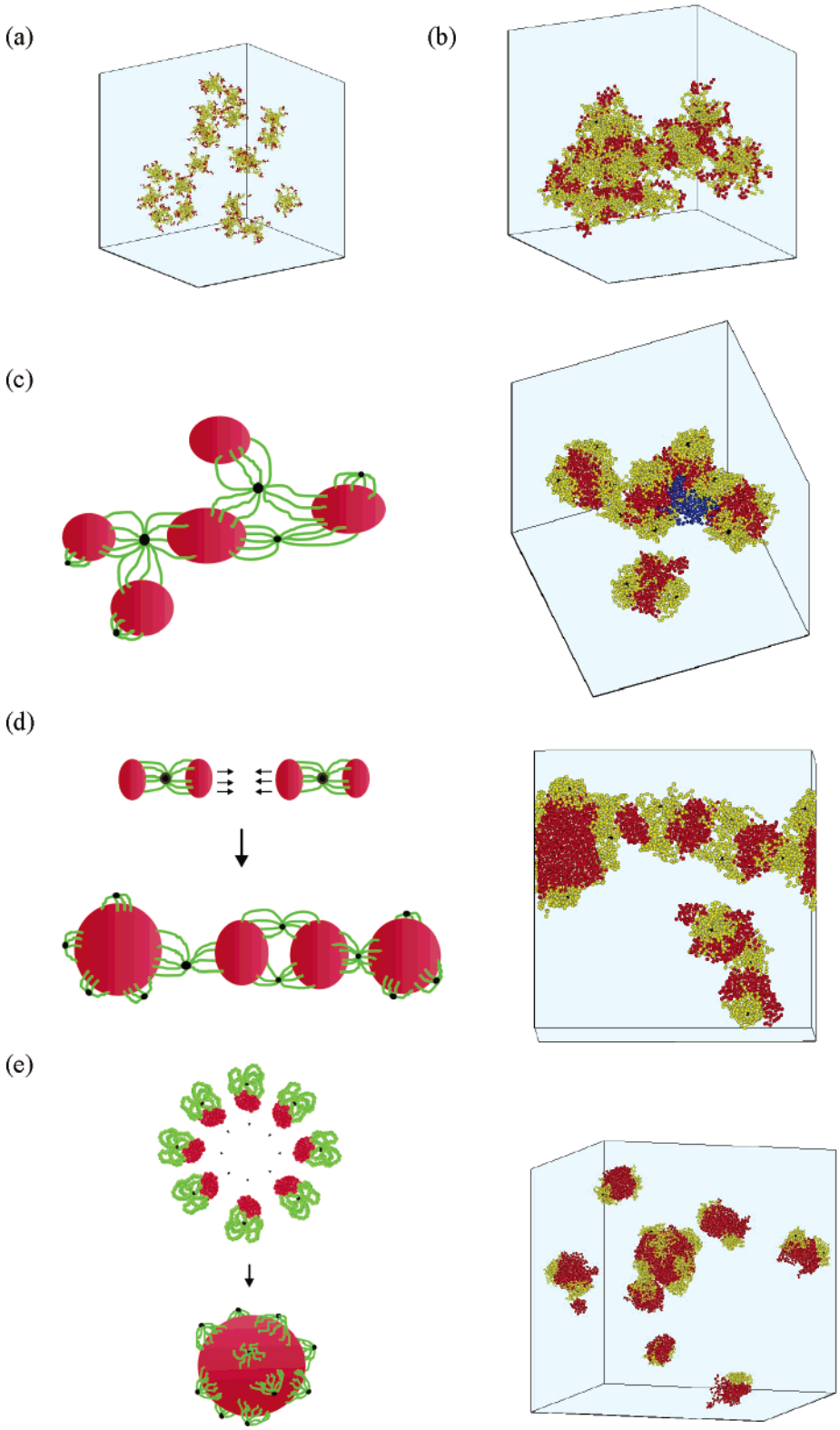

Figure 6. Morphologies of multiple $(AB)_n$ type star-block copolymers in a selective solvent with $L_A = 10$ and (a) $L_B = 3$ (dispersed stars), (b) $L_B = 5$ (connected-star aggregates), (c) $L_B = 10$ (multicore micelles), (d) $L_B = 15$ (segmented worm micelles), and (e) $L_B = 30$ (core-lump micelles). For parts c−e, schematic diagrams of the possible routes for micelle formation are listed. Note that the blue beads shown in part d belong to the same star that interconnects three neighboring cores. All the systems are at a volume fraction of 0.05. The box size actually increases as L_B increases.

single star-block exhibit a freely dispersed manner. As a result, the contacts of *B*-blocks among star-blocks can be easily overcome by thermal motions. The energy reduction due to formation of *B*-block domains is weak compared to conformational and translational entropy. Therefore, as shown in Figure 6a, no micelle formation is observed for a multiple star-blocks system. For $L_B = 5$, a few *B*-domains have developed within a star-block and aggregative behavior begins to disclose. The nanodomains associated with a star-block may be in contact with *B*-domains contributed from different star-blocks, which in turn can associate with other star-blocks. As shown in Figure 6b, a supramolecular structure, called a connected-star aggregate,

is developed by multiple star-blocks. In general, this supramolecule consists of a number of star-blocks that are connected by small *B*-domains. Evidently, its morphology is very different from that of the typical core-corona micelle. The solvent is actually a continuous phase within the aggregate.

When the *B*-block length gets longer, the *B*-block domain grows bigger to avoid contact with solvents. When several star-blocks aggregate together to form a *B*-block core, the topological constraint due to star-block architecture forces *A*-blocks associated with these stars to cover the core. Parts c and d of Figure 6 demonstrate the morphologies of multicore micelles and segmented-worm micelles formed by multiple star-blocks with $L_B = 10$ and 15, respectively. Note that those cores are connected by *A*-blocks. Although both systems display similar supramolecular morphologies, they have a fundamental difference. In the $L_B = 10$ star-block system, the *B*-blocks associated with the same star-block usually belong to three different aggregative *B*-block cores. In other words, the *A*-blocks of the star interconnect three neighboring cores. However, for the $L_B = 15$ star-block system, the *B*-blocks of the same star-block are typically separated into two different cores. This phenomenon can be attributed to the single molecular conformation. As seen in Figure 4, the average number of aggregative *B*-domains is about three for $L_B = 10$ and two for $L_B = 15$. This means that most of the time, a single star-block possesses three ($L_B = 10$) or two ($L_B = 15$) aggregative *B*-block domains. These *B* nanodomains then attract those from other star-blocks to form *B*-block cores, resulting in the event that three or two *B*-block cores share the same star. Therefore, in general, the star-blocks with three aggregative domains ($L_B = 10$) form a multicore conformation, as illustrated in Figure 6c. Star-blocks with two aggregative domains ($L_B = 15$) form a wormlike conformation, as illustrated in Figure 6d.

When $L_B = 30$, the single star-block conformation becomes Janus-like. Our previous Monte Carlo study of heteroarm star copolymers[20] has shown that the formation of Janus structures in individual stars may facilitate the association process and speed up the micellization kinetics. Consequently, it is anticipated that the star-blocks with $L_B = 30$ can also self-assemble to form multimolecular micelles, as shown in Figure 6e. In this case, the *B*-blocks of a star-block are rarely shared between different micelles. As a result, unlike $L_B = 10$ and 15, there is no interconnection between separated cores. In addition, unlike micelles formed by linear diblock copolymers possessing collapsed cores and hairy coronas, the solvophilic *A*-blocks can only take shape as several lumps distributed on the surface of the micellar core due to the topological restriction of the star configuration, as depicted in the schematic representation of Figure 6e.

IV. Conclusion

We have performed mesoscopic simulations, dissipative particle dynamics, to explore the morphologies of star-block copolymers in dilute solutions. In a selective solvent for *A*-block, the solvophobic *B*-blocks are situated in the inner part of the star for $(BA)_n$ but located in the periphery for $(AB)_n$. Due to this difference in the position of the solvophobic block, the single molecular conformation of the $(AB)_n$ type star-block is quite different from that of the $(BA)_n$ type star. As a result, the tendency of forming micelle and the supramolecular structures is different between the two types.

For a star-block copolymer of $(BA)_n$ type, the *B*-blocks attract each other and collapse into a core. This solvophobic core is then surrounded by the solvophilic *A*-block, which form the hairy corona. This single molecular morphology of the $(BA)_n$ star-block copolymer is very similar to the micelle self-assembled by linear *AB* diblock copolymers. Therefore, a $(BA)_n$ type star-block with a large enough arm number such as $n = 14$ can form a stable, unimolecular micelle. The hairy corona provides sufficient steric protection, thus the contact between two *B*-block cores is prevented. Owing to the effective repulsion between $(BA)_{14}$ stars, the multimolecular micelles cannot be formed and the solution contains unimolecular micelles. When the arm number n is small or the solvent is close to the θ condition for the *A*-block, however, association of $(BA)_n$ type star-blocks is still possible. Our simulation results can explain both experimental observation and Brownian dynamics simulation.

For a star-block copolymer of $(AB)_n$ type, a few aggregative domains develop on the periphery of the molecule. As the length of *B*-blocks or the repulsive interaction between *B*-block and solvent is increased, the tendency of *B*-blocks to aggregate within the star increases and thus the average number of aggregative domains declines. When the *B*-block length is long enough, all *B*-blocks favor collapse into one domain and the intramolecular Janus conformation is observed. The exposure of the *B*-domain indicates that a star-block with long solvophobic blocks is not stable and tends to form aggregates with other star-blocks. However, the morphology of the aggregate differs from that of a typical core-corona micelle and is closely related to single molecular conformation. When the star-block conformation possesses two aggregative *B*-domains, a segmented-worm morphology can be observed. For Janus-like conformation, the morphology of the micelle is a solvophobic core with several solvophilic lumps distributed on the surface. Our simulation results indicate that the task of controlling the morphology of the star-block aggregate can be achieved by adjusting the length of the solvophobic block or by altering the solvent.

Acknowledgment. This research is supported by National Council of Science of Taiwan. Computing time provided by the National Center for High-Performance Computing of Taiwan is gratefully acknowledged.

References and Notes

(1) Meier, M.; Gohy, J.; Fustin, C.; Schubert, U. *J. Am. Chem. Soc.* **2004**, *126*, 11517.
(2) Haag, R. *Angew. Chem., Int. Ed.* **2004**, *43*, 278.
(3) Liu, M.; Kono, K.; Frechet, J. *J. Controlled Release* **2000**, *65*, 121.
(4) Anastasiadis, S.; Retsos, H.; Pispas, S.; Hadjichristidis, N.; Neophytides, S. *Macromolecules* **2003**, *36*, 1994.
(5) Heise, A.; Hedrick, J.; Frank, C.; Miller, R. *J. Am. Chem. Soc.* **1999**, *121*, 1.
(6) Pispas, S.; Hadjichristidis, N.; Potemkin, I.; Khokhlov, A. *Macromolecules* **2000**, *33*, 1741.
(7) Ishizu, K.; Uchida, S. *Prog. Polym. Sci.* **1999**, *24*, 1439.
(8) Hadjichristidis, N.; Pitsikalis, M.; Pispas, S.; Iatrou, H. *Chem. Rev.* **2001**, *101*, 3747.
(9) Pitsikalis, M.; Pispas, S.; Mays, J.; Hadjichristidis, N. *Adv. Polym. Sci.* **1998**, *135*, 1.
(10) Heise, A.; Hedrick, J. L.; Frank, C. W.; Miller, R. D. *J. Am. Chem. Soc.* **1999**, *121*, 8647.
(11) Nguyen, A. B.; Hadjichristidis, N.; Fetters, L. J. *Macromolecules* **1986**, *19*, 768.
(12) Voulgaris, D.; Tsitsilianis, C.; Esselink, F. J.; Hadziiloannou, G. *Polymer* **1998**, *39*, 6429.
(13) Mountrichas, G.; Mpiri, M.; Pispas, S. *Macromolecules* **2005**, *38*, 940.
(14) Kiriy, A.; Gorodyska, G.; Minko, S.; Stamm, M.; Tsitsilianis, C. *Macromolecules* **2003**, *36*, 8704.
(15) Gorodyska, G.; Kiriy, A.; Minko, S.; Tsitsilianis, C.; Stamm, M. *Nano Lett.* **2003**, *3*, 365.
(16) Zifferer, G. *J. Chem. Phys.* **1999**, *110*, 4668.
(17) Di Cecca, A.; Freire, J. *Macromolecules* **2002**, *35*, 2851.

(18) Vlahos, C. H.; Horta, A.; Hadjichristidis, N.; Freire, J. J. *Macromolecules* **1995**, *28*, 1500.
(19) Havránková, J.; Limpouchová, Z.; Procházka, K. *Macromol. Theory Simul.* **2003**, *12*, 512.
(20) Chang, Y.; Chen, W.-C.; Sheng, Y.-J.; Jiang, S.; Tsao, H.-K. *Macromolecules* **2005**, *38*, 6201.
(21) Hoogerbrugge, P. J.; Koelman, J. M. V. A. *Europhys. Lett.* **1992**, *199*, 155.
(22) Español P.; Warren, P. B. *Europhys. Lett.* **1995**, *30*, 191.
(23) Groot, R. D.; Warren, P. B. *J. Chem. Phys.* **1997**, *107*, 15.
(24) Huh, J.; Kim, K. H.; Ahn, C.-H.; Jo, W. H. *J. Chem. Phys.* **2004**, *121*, 4998.